Journal of Chromatography A, 1227 (2012) 194–202

Contents lists available at SciVerse ScienceDirect

Journal of Chromatography A

journal homepage: www.elsevier.com/locate/chroma

New insights in the velocity dependency of the external mass transfer coefficient in 2D and 3D porous media for liquid chromatography

Sander Deridder, Gert Desmet*

Vrije Universiteit Brussel, Department of Chemical Engineering, Pleinlaan 2, 1050 Brussels, Belgium

ARTICLE INFO

Article history:
Received 29 July 2011
Received in revised form
29 December 2011
Accepted 1 January 2012
Available online 11 January 2012

Keywords:
Mass transfer
Computational fluid dynamics
Packed bed
Monolith
TSM

ABSTRACT

Numerical calculations of the mobile zone mass transfer rate in a variety of ordered 2D and 3D structures are presented. These calculations are in line with earlier theoretical and experimental findings made in the field of chemical engineering and suggest that the Sherwood-number (Sh_m) appearing in the mobile phase mass transfer term of the general plate height expression of liquid chromatography is not correctly predicted by the Wilson–Geankoplis – or the Kataoka – or the penetration model expression that have been used up to now to in the field of LC, and that at least more research is needed before these expressions can be continued to be used with confidence. The aforementioned expressions were obtained by neglecting the effect of axial dispersion on the mass transfer process, and it seems that they therefore underestimate the true Sh_m-number by a factor of 2–5 around the minimum of the van Deemter-curve. New correlations describing the variation of the Sh_m-coefficient as a function of the reduced velocity for a number of other packing geometries (tetrahedral monolith, 2D pillar array) are proposed. These correlations are in agreement with earlier theoretical and experimental studies showing that at low velocities the local-driving force-based Sh_m-value is of the order of 10–20 in a packed bed column with an external porosity on the order of 35–40%.

1. Introduction

The general plate height model, originally introduced by Lapidus and Amundson [1] and later used by van Deemter et al. and other researchers for the specific application of liquid chromatography [2–7], is generally accepted as the standard model for the band broadening in packed and monolithic chromatography media. Many variants of the general plate height model exist (resulting from the use of different notations and parameter definitions), but they can all be reduced to an expression of the following form [8]:

$$h = h_{inhom} + \frac{2\gamma_{eff}(1+k'')}{\nu_i} + 2\frac{k''^2}{(1+k'')^2}\frac{\nu_i}{\alpha}\frac{1}{Sh_m}\frac{\varepsilon}{1-\varepsilon} + 2\frac{k''}{(1+k'')^2}\frac{\nu_i}{\alpha}\frac{1}{Sh_{part}}\frac{D_{mol}}{D_{part}} \quad (1)$$

wherein ν_i is the reduced interstitial velocity (defined as $\nu_i = u_i d/D_{mol}$), h_{inhom} represents the band broadening contributions arising from the heterogeneity of the bed, γ_{eff} is the effective longitudinal diffusion ($\gamma_{eff} = D_{eff}/D_{mol}$), and Sh_m and Sh_{part}, respectively, are the dimensionless mobile zone and particle zone mass transfer coefficient (Sh = Sherwood-number). In addition, α is a shape factor ($\alpha = 6$ for spherical particles and 4 for infinitely long cylinders) and k'' is the zone retention factor (related to the t_0-based retention factor k' via $k'' = (1+k')\varepsilon_T/\varepsilon - 1$, wherein ε_T and ε, respectively, are the total and the external bed porosity). Similarly, the interstitial reduced velocity (ν_i) is related to the more easily accessible t_0-based reduced velocity (ν_0) via $\nu_i = \nu_0(\varepsilon_T/\varepsilon)$.

Although physically and mathematically sound, the general plate height model is based on a number of approximations and assumptions such as the fact that the velocity profile in the interstitial through-pores is flat (plug flow) and the fact that the different contributing band broadening sources are independent of each other. The validity of these assumptions is difficult to check experimentally, because Eq. (1) contains a number of parameters (Sh_m, γ_{eff} and D_{part}) whose value is ill-known under experimental conditions [9,10]. In addition, some of the terms in Eq. (1) contain velocity-dependent parameters (h_{inhom} and Sh_m) that need to be estimated using empirical or semi-empirical correlations. The h_{inhom}-term for example is typically modeled via one or more so-called Giddings-coupling terms [6,11,12]. However, the parameters needed in these Giddings-couplings terms are a priori unknown and need to be determined by curve fitting Eq. (1) to a set of experimental data.

In an attempt to reduce the uncertainty on the different terms appearing in Eq. (1), the present study focuses on the mobile zone mass transfer term (3rd term on right hand side). This term

* Corresponding author. Tel.: +32 02 629 32 51; fax: +32 02 629 32 48.
E-mail address: gedesmet@vub.ac.be (G. Desmet).

0021-9673/$ – see front matter © 2012 Elsevier B.V. All rights reserved.
doi:10.1016/j.chroma.2012.01.007

contains a parameter, Sh_m, which is nothing else but the dimensionless version of the mobile zone mass transfer coefficient (k_m), generally defined as:

$$Sh_m = \frac{k_m d}{D_{mol}} \quad (2)$$

wherein d is the characteristic size of the packing or the tube.

Nomenclature

a	specific contact area [m^{-1}]
A	Giddings coupling-term parameter (see Eq. (14))
B	dimensionless B-term
C	concentration [kg/m^3]
C_{in}	inlet concentration [kg/m^3]
C_m	mobile zone concentration [kg/m^3]
C_{out}	outlet concentration [kg/m^3]
C_s	static zone concentration [kg/m^3]
d	characteristic size of the packing or tube [m]
D	Giddings coupling-term parameter (see Eq. (14))
D_{ax}	axial dispersion coefficient [m^2/s]
D_{mol}	molecular diffusion coefficient in the mobile zone [m^2/s]
D_{part}	molecular diffusion coefficient in the static zone [m^2/s]
d_{tube}	tube diameter [m]
h	reduced plate height
h_{ax}	axial dispersion contribution to the reduced plate height
h_{Cm}	contribution of mobile zone mass transfer to the dimensionless plate height
h_{eddy}	contribution of eddy dispersion to the dimensionless plate height
k''	zone retention coefficient
k_m	mobile zone mass transfer coefficient [m/s]
$k_{m,ln}$	apparent mass transfer coefficient [m/s]
K_p	particle based equilibrium constant
L	length between inlet and outlet [m]
Re	Reynolds number ($=u_0 d/\nu$)
S	total contact area [m^2]
Sc	Schmidt number ($=\nu/D_{mol}$)
Sh_m	dimensionless mobile zone mass transfer coefficient or Sherwood number (see Eq. (2))
Sh_{part}	dimensionless static zone mass transfer coefficient or Sherwood number (see Eq. (2))
t_0	retention time of an unretained component [s]
u_i	interstitial velocity [m/s]
V	volume [m^3]
x	distance in the flow direction [m]

Greek symbols

α	shape factor (=6 for spherical particles, =4 for infinitely long cylinders)
ε	external porosity
ε_T	total porosity
ϕ	mass flux to the surface [$kg/(m^2\ s)$]
γ_c	shape factor
γ_d	shape factor
ν	kinematic viscosity [m^2/s]
ν_0	reduced chromatographic velocity
ν_i	reduced interstitial velocity

Sh_m generally varies with the mobile phase velocity. In the field of LC, this dependency is often represented via the Wilson–Geankoplis equation [6,13–15]:

$$Sh_m = \frac{1.09}{\varepsilon^{2/3}} \nu_i^{1/3} \quad (3)$$

In some cases [8,10,16,17], other correlations, such as the Kataoka or the penetration model are being used. All of them are, however, of the same form, which can be written as:

$$Sh_m = Y_c \nu_i^n \quad \text{with } 1/3 < n < 1/2 \quad (4)$$

In previous publications [8,18,19], our group has criticized such mobile zone mass transfer expressions. Indeed, as it implies that Sh_m tends to zero when the velocity tends to zero, the form of these expressions suggests that the mass transfer would stop when the velocity stops. This seems to be physically invalid and it was therefore proposed in [8] to add a constant term to Eq. (4):

$$Sh_m = \gamma_d + \gamma_c \nu_i^n \quad (5)$$

Using Eq. (5), it was possible to prove the general plate height model described by Eq. (1) to be accurate to within a few percent. Using only one set of geometrical shape factors (the γ_c and γ_d-parameters appearing in Eq. (5)) completed with two Giddings-parameters to represent the velocity dependency of h_{inhom} (see Eq. (14) further on), it was possible to closely fit Eq. (1) to a set of highly accurate plate height data over a broad range of velocities, retention factors, and values of the intra-particle diffusion coefficient [18,19]. Because the data were generated via numerical simulation, the actual value of the diffusion constants in the interstitial and the stationary zone was exactly known. In a real-world experiment, these diffusion constants are only known approximately and the uncertainty on their value inevitably masks any fitting or modeling errors. In a numerical test, this uncertainty is not present, making the fitting test much more stringent than in a real experiment. The good agreement between model and simulated data obtained in [18,19] showed that the general plate height model works very well when used with an expression for k_m of the form given by Eq. (5), despite the apparently crude underlying approximations (e.g., plug flow in the interstitial pores).

In the present study, it is attempted to validate Eq. (5) in an independent way, by directly measuring Sh_m via the local mass transfer flux instead of estimating its value indirectly as was done in [18,19]. Whereas very difficult to realize in practice, the local mass transfer rate can relatively easily be determined when doing computer simulations, as in this case the concentration field is exactly known at any location of the bed. Similar to the work in [19], the data are again generated on a series of perfectly ordered 2D and 3D media, as these can be calculated within a reasonable time frame (due to the many symmetries and periodic planes that can be used, the actual flow domain that needs to be calculated can be strongly reduced). An additional advantage of ordered structures is that they should lead to Sh_m-values that are periodically constant, hence offering an additional means to check the accuracy of the calculations. The procedure to determine the Sh_m-values was first validated on a simplified case (mass transfer to the inner wall of a cylindrical tube), as in this case the value for Sh_m is exactly known analytically [20].

2. Background theory and literature on mobile zone mass transfer

Before starting the actual study, it should first be considered that the literature concerning the local mass transfer coefficient in packed bed columns is often contradictive and confusing. As clearly demonstrated by Fedkiw and Newman [21,22] and by Wakao et al. [23], this is largely due to the co-existence of two different definitions for the mass transfer coefficient.

The first mass transfer coefficient, further denoted by k_m, directly represents the local mass transfer conditions and is the coefficient that appears in the uni-dimensional mass balance of a dissolved species subjected to axial convection and dispersion, as well as to a transversal mass transfer process to a solid zone or interphase kept at $C = 0$:

$$-u_i \frac{dc}{dx} + D_{ax} \frac{d^2c}{dx^2} = a k_m C \quad (6)$$

In Eq. (6), a is the specific contact area (solid surface over liquid volume) between the fluid and the solid. Eq. (6) is also of the same type as the mass balance leading to the general plate height model given by Eq. (1). The only difference between Eq. (6) and the mobile zone mass balance leading to Eq. (1) is that the right hand side of the expression should be changed from $k_m aC$ to $k_m a(C_m - C_s/K_p)$ to express that the mass transfer between the mobile and stationary zone in chromatography is reversible and tends to an equilibrium state where $C_s = K_p C_m$.

The second mass transfer coefficient, very popular in the typical chemical engineering literature, and further denoted by $k_{m,ln}$, links the observed concentrations at the inlet and outlet of the bed (resp. C_{in} and C_{out}) during a mass transfer experiment such as, for example, the measurement of the uptake of benzoic acid in a water stream from pure benzoic acid particles as was the case in the classic experiment of Wilson and Geankoplis [13]. The interpretation of this second type of mass transfer coefficient is based on the assumption that the axial dispersion term in Eq. (6) can be neglected, so that:

$$k_{m,ln} = \frac{u_i}{aL} \ln\left(\frac{C_{in}}{C_{out}}\right) \quad (7)$$

whereas the k_m-coefficient needed in Eq. (6) requires the measurement of the local mass transfer fluxes and concentrations, the $k_{m,ln}$-coefficient needed in Eq. (7) is readily accessible via a simple external measurement of C_{in} and C_{out}. This explains why most of the experimental literature studies, including that of Wilson and Geankoplis, report $k_{m,ln}$ and not k_m.

When the second term (axial dispersion term) on the left hand side of Eq. (6) can be neglected, Eq. (7) is the solution to Eq. (6) and the difference between k_m and $k_{m,ln}$ vanishes. However, when the axial dispersion term becomes important (which is the case when the velocity drops below a certain limit, as it does in liquid chromatography), the two values start to strongly deviate. When the reduced velocity tends to zero, the two different definitions even tend to a different limit. Whereas $k_{m,ln}$ tends to zero when $\nu_i \to 0$, the k_m-coefficient tends to a finite value, and is thus significantly larger than $k_{m,ln}$ [21,22,24]. According to Fedkiw and Newman [21,22], the deviation between the two expressions already becomes significant when $\nu_i < 50$. The effect is hence important over the whole range of relevant reduced chromatographic velocities.

In the famous Wilson and Geankoplis [13] paper, the authors used liquids with a Schmidt-number of 50,000–70,000, i.e., 50–70 times higher than in normal liquids. The lowest Reynolds point in Fig. 3 of their paper, which is a point that in fact already starts to get off the experimental correlation line, corresponds to a reduced chromatographic velocity of 75 ($\nu_0 = Re\,Sc = 0.0015 \times 50{,}000 = 75$). The authors also used water as mobile phase in their experiments and in that case the lowest Reynolds point corresponds to a reduced chromatographic velocity of 40 ($\nu_0 = Re\,Sc = 0.04 \times 1000 = 40$). In both cases, the lowest ν_0-value they considered lies around the $\nu_0 > 50$ criterion of Fedkiw and Newman [21,22] above which the axial dispersion is indeed negligible. Hence, considering that most chromatographic separations occur in the $\nu_0 = 5$–20 range, one should realize that the Wilson and Geankoplis correlation is only valid well outside this range.

Furthermore considering that Eq. (1) is based on the same type of mass balance as Eq. (6), it should be clear that the mass transfer coefficient needed in the general plate height model should be the k_m-variant, i.e., that based on the local flux and the local driving force (cf. Eq. (6)) and not the $k_{m,ln}$-variant. Unfortunately, this is the type of mass transfer coefficient used in the two most frequently employed Sherwood correlations in the field of chromatography: the Wilson and Geankoplis- and the Kataoka-correlation [10,25].

Whereas the latter correlations tend to zero in the $\nu_i \to 0$-limit, experimental literature data collected and interpreted under the correct definition (i.e., by taking the effect of axial dispersion into account) consistently show that the k_m- and Sh_m-values can be expected to be finite (of the order of 10–20) in the $\nu_i \to 0$-limit. Miyauchi et al. [26] found, using electrical current density measurements, a value around $Sh_m = 15$ in the $\nu_i \to 0$-limit for a sphere packing with an external porosity around $\varepsilon = 0.47$. Gunn and Souza [27] found a value around $Sh_m = 10$ in the $\nu_i \to 0$-limit for the gas phase mass transfer in a more densely packed bed. Both values furthermore agree well with the theoretical value of around 12 that was predicted theoretically by Pfeffer and Happel [28], using a free-surface model to calculate the local mass transfer rate to a sphere in a randomly packed bed.

Another, often ignored, shortcoming of the Wilson and Geankoplis-correlation is that it was obtained under so-called diluted bed conditions. This means that only a fraction of the spheres suspended in the bed were active in the Wilson–Geankoplis study [13]. In this way, the influence of the neighboring particles on the driving force for mass transfer is underestimated [29]. Therefore, Sh-values obtained in diluted beds cannot be used in undiluted beds, like chromatographic columns [29].

3. Numerical methods and considered geometries

To cover the broadest possible range of existing chromatographic bed geometries, the mass transfer rate has been calculated for 4 different general geometrical classes: a cylindrical tube (as employed in open-tubular liquid chromatography [30,31] and used here for validation purposes as this is a case for which the analytical solution is known [20]); a 2D equilateral triangular array of cylindrical pillars (see Fig. 1a) to represent the pillar array columns developed by our group and others [32–34]; a 3D ordered monolithic skeleton structure (tetrahedral skeleton model [34–37], see Fig. 1b) as a first principle approximation to the typical packing structures encountered in monolithic columns; finally an ordered array of spheres (face centered cubic (fcc) packed, see Fig. 1c for a 3D representation of the structure) to represent the case of an (ordered) packed bed column. For the monolith geometry, two different external porosities were considered: one corresponding to a typical packed bed value (for which external porosity $\varepsilon = 0.38$), and a larger one to investigate the impact of the external porosity of the packing ($\varepsilon = 0.60$). For the ordered array of spheres, four geometries with different porosities ranging from $\varepsilon = 0.35$ to $\varepsilon = 0.44$ were considered. Besides these cases, one substantially higher porosity ($\varepsilon = 0.80$) was considered as well.

The cylindrical tube was drawn as a rectangle on which an axisymmetry boundary condition was installed on one long edge and a wall boundary condition on the other. Pressure inlet and outlet boundary conditions were applied on the boundaries in the flow direction (short edges). The other structures display symmetry and/or periodicity in the x-, y- and z-direction. Therefore it is possible to draw a unit cell for each considered structure. This unit cell can reconstitute the original structure by proper reflection and/or translation. Symmetry or periodic boundary conditions were applied to the boundaries in the y- and z-direction (perpendicular to the flow direction). Although the structures also display

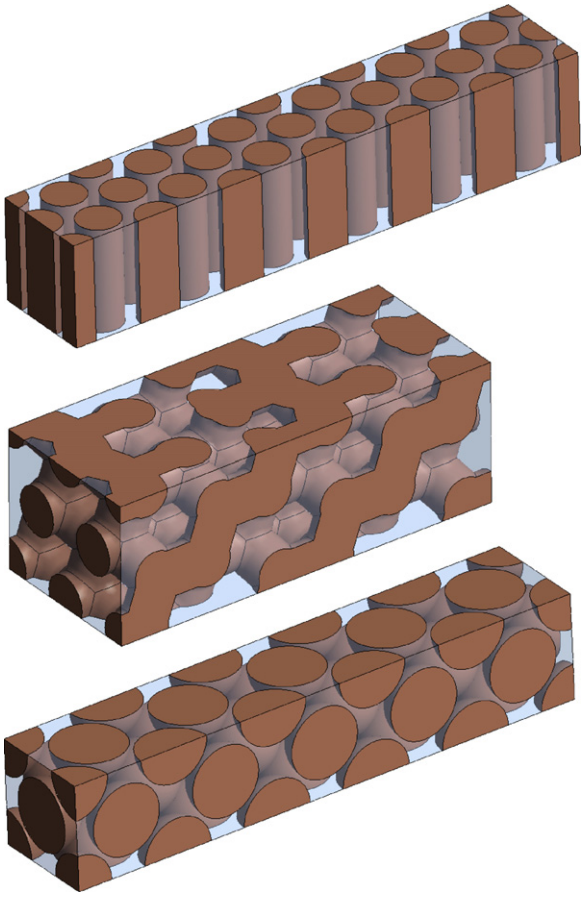

Fig. 1. Unit cell (not the smallest possible) of (a) an equilateral triangular array of cylindrical pillars ($\varepsilon = 0.40$), (b) the Tetrahedral Skeleton Model monolith ($\varepsilon = 0.38$) and (c) an array of face centered cubic ordered spheres ($\varepsilon = 0.38$).

a periodicity in the x-direction (flow direction), the expected concentration field does not. Therefore, the unit cells were mirrored or translated several times in the x-direction. Pressure inlet and outlet boundary conditions were installed on the boundaries in the flow direction.

The cylindrical tube was meshed using 175,000 triangular cells. This mesh was deliberately meshed with triangular cells to facilitate comparison with the equilateral triangular array of cylinders (which was also meshed using triangular cells). A sizing function (growth rate = 1.15) was attached to the cylinder wall. The maximum cell skew never exceeded 0.37. The face centered cubic sphere packing was meshed using on the order of 2,000,000 tetrahedral cells. A boundary layer mesh was attached to the monolith wall. This layer consisted of triangular prism (or wedge shaped) cells arranged in 5 layers, with a layer thickness growth rate of 1.2. A sizing function was attached to the particle walls (growth rate = 1.15). The maximum cell skew never exceeded 0.88 and the average cell skew ranged from 0.17 to 0.20. The TSM monolith was meshed using 1,400,000–2,800,000 tetrahedral cells (depending on the external porosity resulted in slightly different cell numbers). A sizing function was attached to the monolith walls (growth rate = 1.25). The maximum cell skewness never exceeded 0.90 and the average cell skew ranged from 0.27 to 0.28. The equilateral triangular array of cylinders was meshed using 240,000 triangular cells. A sizing function was attached to the cylinder walls (growth rate = 1.15). The maximum cell skew was 0.40.

Flow and convection-diffusion equations were solved using a second order upwind discretization scheme, applying a species sink condition (constant zero concentration) at the interior wall surfaces, and using constant (non-zero) concentration at the pressure inlet. Since Eq. (6) is a steady-state equation, the problem could be solved in the steady-state mode.

Once the steady-state concentration profiles were calculated, the reporting function of the software was used to calculate the surface-averaged species flux at the chromatographic surfaces (nominator of Eq. (8)) and the volume-averaged species concentration (denominator of Eq. (8)):

$$k_m = \frac{(1/S)\int \phi \, dS}{(1/V)\int C \, dV} \tag{8}$$

wherein ϕ is the total mass flux to the surface in the considered control volume and wherein V and S resp. are the liquid volume and total contact area in the same control volume.

Grid checks were performed until the change with the previous solution for Sh_m was less than 0.5%. This criterion was checked for the three different geometries for one porosity value and several ν_i-values. Sizing functions were used to ensure smaller grid cells near the stationary phase boundaries, because the highest velocity- and concentration-gradients occur in these regions.

4. Results and discussion

4.1. Concentration profiles and accuracy of the numerical results

Fig. 2 shows the calculated steady-state species concentration profiles in the four considered different geometries. At the inlet, the species are introduced at a concentration $C = 1$ (colour code = red). Since the solid zone boundaries are kept at $C = 0$ (and hence "consume" the species), it is straightforward to observe that the regions close to the solid walls are coloured blue (very low concentration)

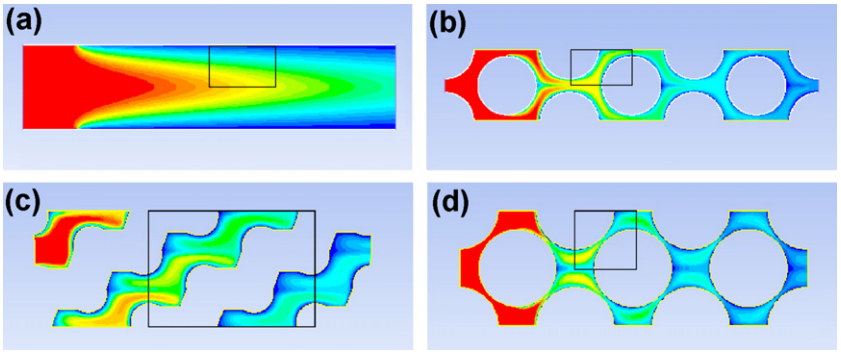

Fig. 2. Calculated species concentration fields in the axisymmetrical plane of (a) a cylindrical tube, (b) a 2D array of cylindrical pillars, (c) a 3D monolithic skeleton structure (tetrahedral skeleton model, see Fig. 1b for a 3D representation of the structure) with external porosity $\varepsilon = 0.38$, and (d) an ordered array of spheres (fcc packed, see Fig. 1c for a 3D representation of the structure).

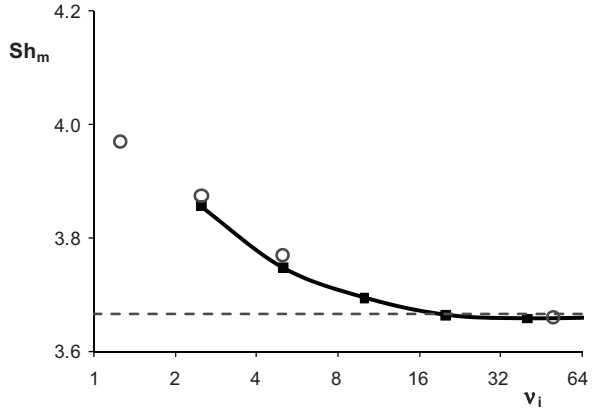

Fig. 3. Variation of Sh_m as a function of the dimensionless velocity ν_i for the case of a cylindrical tube (■). The dashed horizontal line represents Eq. (9). The open circle data points represent the analytical solution of Papoutsakis et al. [20].

and that the colour changes from red (inlet) to blue (outlet) as the concentration gradually decreases along the longitudinal axis as the species disappears at the solid boundaries.

Because the studied flow domains can be considered as a series connection of identical unit cells (see black boxes added to Fig. 2), and since the average Sh_m-value should be the same in every unit cell, the possibility to investigate whether the value of Sh_m varies remains the same in each unit cell provides an important internal accuracy check. This was deemed important, especially for the case of low reduced velocities, because in this case the concentration very rapidly drops (more than 5 orders of magnitude per unit cell), potentially leading to numerical errors on the determination of the average flux and concentration in the most downstream unit cells. Another problem that needed to be considered is the existence of an entrance region, where the velocity and concentration gradients are developed into the profiles they display in the rest of the bed. Inevitably, the mass transfer in this region is different from that in the rest of the bed. According to the theory of heat and mass transfer, the mass transfer coefficients are larger in this entrance region [38].

This was also observed in our simulations, as the Sh_m-values in the first unit cell were consistently larger than in the following unit cells. For the high ν_i-case in the cylindrical tube, the entrance region even persists over the first 3 unit cells. The last cells of the considered flow domains also lead to a deviating value, mainly because the concentration in these cells becomes so small that the uncertainty on the determination of the average wall flux and concentration becomes too large. The results of these cells were therefore not taken into account. Also the value in the entrance region was not considered. The Sh_m-values reported in the present study were calculated in the region between the entrance and exit region, where the Sh_m-value never varied by more than 0.5% over at least three consecutive unit cells. When such a region could not be detected, i.e., when the velocity was either too large or too small, the simulations were stopped. This is also the reason why different velocity ranges are being covered in Figs. 3–6.

Fig. 3 shows how Sh_m varies with the reduced velocity in the cylindrical tube case. The literature value that is usually cited for Sh_m in cylindrical pipe with uniform cross-section is independent of the reduced velocity and is given by:

$$Sh_m = \frac{k_m d_{tube}}{D_{mol}} = 3.66 \quad (9)$$

As can be noted from Fig. 3, the data computed via the employed numerical methods correspond exactly to this value in the large ν_i-range (cf. the agreement with the dashed horizontal line). For

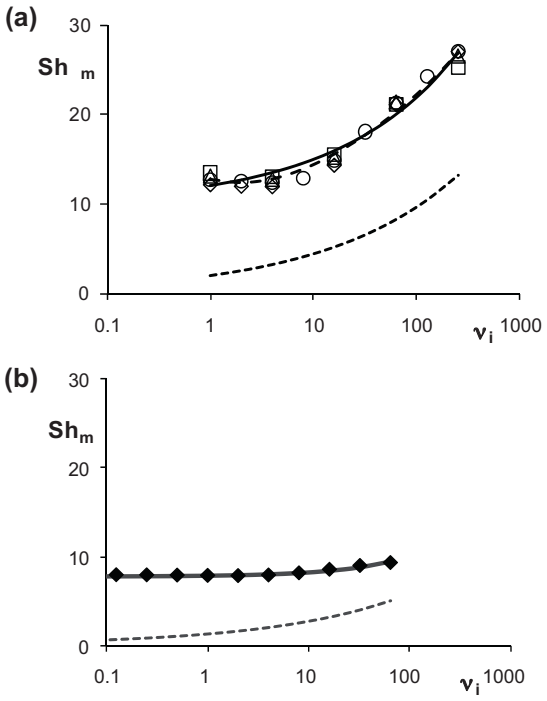

Fig. 4. Variation of the computed Sh_m-values as a function of the dimensionless velocity ν_i for the case of a 3D array of spheres with external porosity (a) $\varepsilon = 0.35$ (◊), $\varepsilon = 0.38$ (○), $\varepsilon = 0.41$ (△), $\varepsilon = 0.44$ (□) and (b) $\varepsilon = 0.80$. The solid line corresponds to Eq. (10), the long dashed line to Eq. (11). The dashed line represents the Wilson–Geankoplis correlation (Eq. (3)).

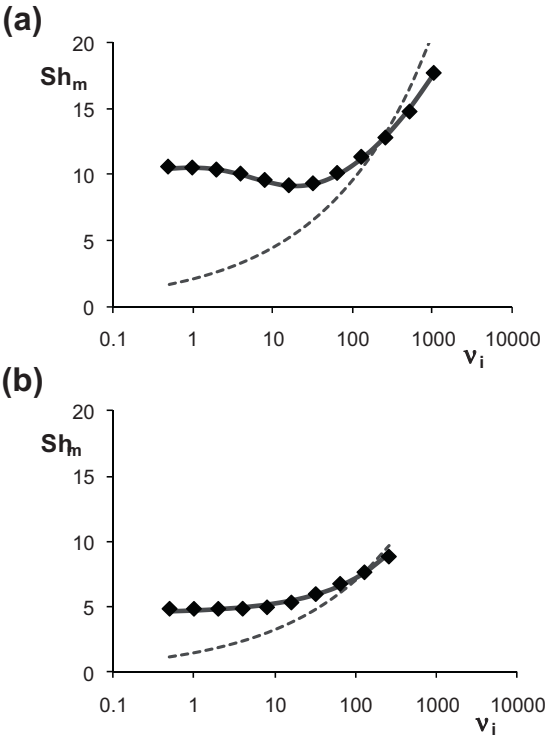

Fig. 5. Variation of Sh_m as a function of the dimensionless velocity ν_i for the case of a monolithic column mimic (TSM) with external porosity (a) $\varepsilon = 0.38$ and (b) $\varepsilon = 0.60$. The solid line corresponds to Eq. (12). The dashed line represents the Wilson–Geankoplis correlation (Eq. (3)).

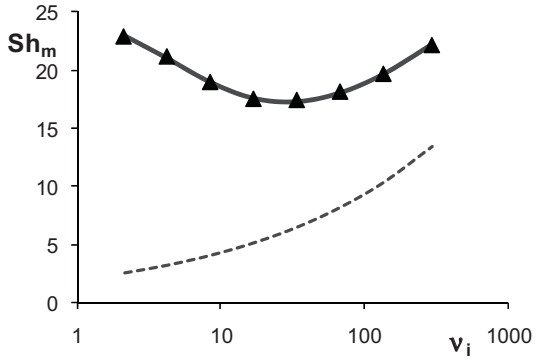

Fig. 6. Variation of Sh_m as a function of the dimensionless velocity ν_i for the case of a 2D pillar array with external porosity $\varepsilon = 0.40$. The solid line corresponds to Eq. (13). The dashed line represents the Wilson–Geankoplis correlation (Eq. (3)).

smaller ν_i-values, the computed data points deviate from this value and increase with decreasing ν_i. The computed data, however, still are in full agreement with the analytical solution to the extended Graetz-problem established by Papoutsakis et al. (gray open circles), showing that Eq. (6) only holds in the large ν_i-range [20] and that, when ν_i drops below 20, Sh_m no longer remains constant but gradually increases with ν_i when ν_i decreases.

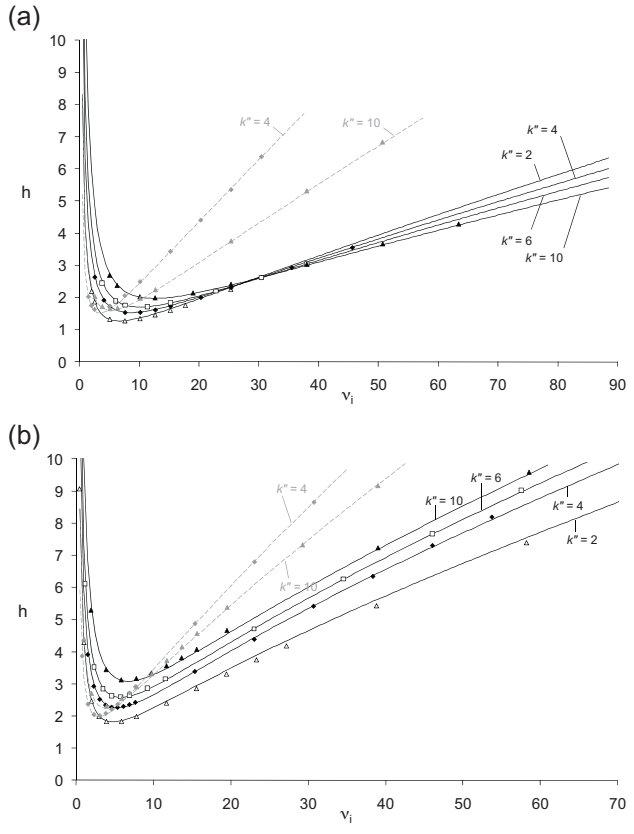

Fig. 7. Plate height values (symbols) obtained via the numerical study presented in [18] for different values of ν_i and the zone retention factor k'' and best-fit (lines) with Eqs. (1) and (14), using the Sh_m-values computed in the present study and a best-fit of A and D needed in Eq. (14). Black lines and symbols: $D_{part} = 5 \times 10^{-10}$ m^2/s; gray lines and symbols: $D_{part} = 1 \times 10^{-10}$ m^2/s ($D_{mol} = 1 \times 10^{-9}$ m^2/s in both cases). (a) TSM-case with $\varepsilon = 0.38$; (b) TSM-case with $\varepsilon = 0.60$.

4.2. Variation of Sh_m as a function of the reduced velocity for the various packed bed structures

Fig. 4a and b shows the volume-average concentration-based Sh_m-values in the five considered sphere arrays. As can be noted, Sh_m increases with ν_i for ν_i larger than 10, whereas Sh_m reaches a constant value when ν_i becomes smaller than this value and tends to zero. In other words, the computed Sh_m-data do not vary with ν_i according to a correlation of the form of Eq. (4) but rather follow a correlation of the form represented by Eq. (5):

$$Sh_m = 9.9 + 2.1\nu_i^{0.37} (0.35 < \varepsilon < 0.44) \quad 1 < \nu_i < 250 \tag{10a}$$

$$Sh_m = 7.8 + 0.090\nu_i^{0.69} (\varepsilon = 0.80) \quad 0.06 < \nu_i < 60 \tag{10b}$$

In the low porosity cases ($0.35 < \varepsilon < 0.44$, see Fig. 4a), the agreement between Eq. (10a) and the computed data (open symbols) is not perfect (cf. the solid line). A better fitting of the data can be obtained using the following expression (cf. the long dashed line):

$$Sh_m = \frac{13}{1 + 2.1\nu_i} + 8.6\nu_i^{0.21} (0.35 < \varepsilon < 0.44) \quad 1 < \nu_i < 250 \tag{11}$$

The particularity of Eq. (11) is that it allows to represent the slight increase of Sh_m with decreasing ν_i between $\nu_i = 1$ and $\nu_i = 10$, a phenomenon that is similar to that already observed in the cylindrical tube case represented in Fig. 3.

The Wilson–Geankoplis expression (represented by the dashed line) on the other hand clearly fails to represent the computed data. As discussed in Section 2, this is due to the fact that the Wilson–Geankoplis expression is based on the $k_{m,ln}$-coefficient, which is only correct and relevant when used in combination with an expression of the form of Eq. (7) and not when used in combination with a mass-balance of the type of Eq. (6), as is needed to derive general plate height expression of chromatography. The largest discrepancy between the computed Sh_m-data and the Wilson–Geankoplis expression is situated in the range of $\nu_i < 10$, where the former remains constant around a given (high) value, while the other tends to zero. This is most pronounced in the $\varepsilon = 0.8$-case (and also in the other geometries considered further on). This major difference can, according to the theoretical work of Fedkiw and Newman [21,22], be fully attributed to the different influence of the axial dispersion on the Sherwood numbers that are based on k_m (such as the computed data in this study) and those based on $k_{m,ln}$ (as is the case for the Wilson–Geankoplis expression).

In the low ε-case (Fig. 4a), the computed Sh_m-value in the $\nu_i \to 0$-limit approximately equals $Sh_m = 12.7$, which lies very close to the theoretical value of $Sh_m = 12$ predicted by Pfeffer and Happel for a sphere packing with $\varepsilon = 0.40$, using a free surface model which they could solve analytically [28]. This agreement reconfirms the excellent accuracy of the present numerical modeling work. The value also agrees well with the experimental value for Sh_m-reported by Miyauchi et al. [26], who found a value of $Sh_m = 15$ for a sphere packing with a slightly larger external porosity ($\varepsilon = 0.47$). The value of $Sh_m = 12$ also agrees well with the value that would be obtained when extrapolating the extensive data set compiled by Wakao et al. [23] to the $\nu_i \to 0$-limit.

Comparing Fig. 4a with 4b allows assessing the effect of the external porosity on the observed Sh_m-value. Again in agreement with the theoretical calculations of Pfeffer and Happel [28], the Sh_m-values decrease with increasing ε. This is mainly due to the fact that the relevant characteristic length for the mass transfer is not the particle diameter but the size of the through-pores between the particles. Considering a fixed particle size (which is what one does when comparing Sh_m-values that are calculated on the basis of the particle diameter), the through-pores of the $\varepsilon = 0.80$-case are considerably larger than in the low ε-cases. Combining this with the obvious fact that narrower through-pores lead to a higher mass

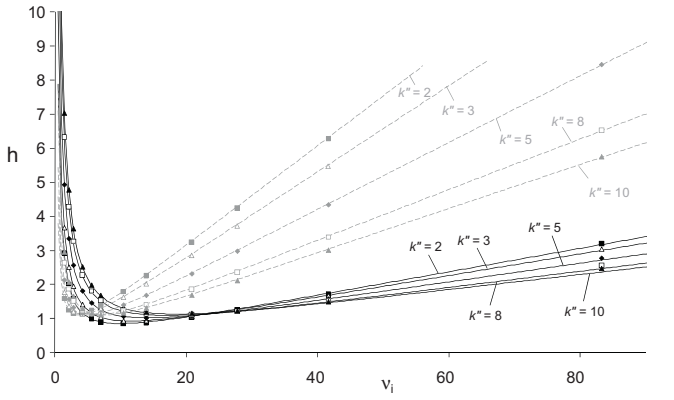

Fig. 8. Plate height values (symbols) in a 2D pillar array obtained via the numerical study presented in [19] for different values of ν_i and the zone retention factor k'' and best-fit (lines) with Eqs. (1) and (14), using the Sh_m-values computed in the present study and a best-fit of A and D needed in Eq. (14). Black lines and symbols: $D_{part} = 5 \times 10^{-10}$ m^2/s; gray lines and symbols: $D_{part} = 1 \times 10^{-10}$ m^2/s ($D_{mol} = 1 \times 10^{-9}$ m^2/s in both cases).

transfer rate (because of the shorter distance that needs to be covered), it is indeed obvious to find that the low ε-cases lead to larger Sh_m-values than the $\varepsilon = 0.80$-case. In fact, all existing correlations and literature expressions (including the Wilson and Geankoplis correlation) predict a similar qualitative dependency of a decreasing Sh_m (or $Sh_{m,ln}$) with increasing ε.

To study the effect of the external porosity in more detail in the region of external porosities typically encountered in a packed bed of spheres, four different porosities ranging from 0.35 to 0.44 were considered. The result is shown in Fig. 4a. As can be noted, the influence of ε is rather small (maximum 10%) in this porosity range. Because of this small difference, the Sh_m-data for the different external porosities in Fig. 4a can all be very closely represented by Eqs. (10a), (10b) and (11).

A similar dependency on the external porosity as observed in Fig. 4 for the sphere array is observed for the 3D Tetrahedral skeleton model (TSM), where the $\varepsilon = 0.38$-case also leads to considerably larger Sh_m-values than the $\varepsilon = 0.60$-case (Fig. 5a and b).

Similarly to what was already apparent for the $\varepsilon = 0.38$-sphere array, the data for the $\varepsilon = 0.38$-TSM do not monotonically decrease when going from large to low ν_i-values (see Fig. 5a). Instead, the Sh_m-values go through a minimum around $\nu_i = 20$ and slightly increase with a further decrease of ν_i until a constant value is reached in the $\nu_i \rightarrow 0$-limit. It is believed this type of increase is of the same nature as the increase of the Sh_m-values observed for decreasing ν_i-values in the cylindrical tube (see Fig. 3). Whereas the $\varepsilon = 0.60$-data can still be represented by an expression of the type of Eq. (5), the $\varepsilon = 0.38$-data can only be fitted with an adapted expression of the same type as Eq. (11), allowing to account for the fact that Sh_m decreases with increasing ν_i in the small ν_i-range. This, respectively, yields:

$$Sh_m = \frac{8.0}{1 + 0.13\nu_i} + 3.5\nu_i^{0.23} (\varepsilon = 0.38) \quad 0.5 < \nu_i < 1000 \qquad (12a)$$

$$Sh_m = 4.5 + 0.20\nu_i^{0.56} (\varepsilon = 0.60) \quad 0.5 < \nu_i < 250 \qquad (12b)$$

Similar to the 3D sphere array case considered in Fig. 4, the Wilson–Geankoplis expression is again far off, as are all other possible correlations (Kataoka-model, penetration model) of the type given by Eq. (4) (data not represented).

The increase of Sh_m with decreasing ν_i in the range of small ν_i which was already visible in the cylindrical tube case (Fig. 3) and in the sphere array and the TSM with $\varepsilon = 0.38$ (Figs. 4a and 5a) is even more pronounced in the 2D cylinder array (Fig. 6), where the (downward) slope of the Sh_m-curve in the small ν_i-range is nearly

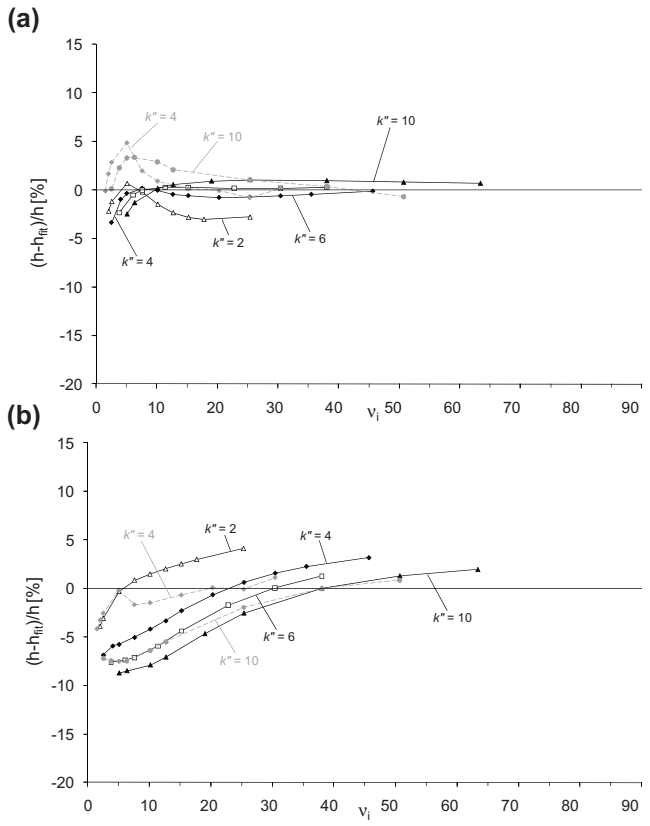

Fig. 9. Relative residual plots for the fitting quality of the TSM ($\varepsilon = 0.38$)-data shown in Fig. 7a using (a) the presently computed Sh_m-values and (b) Sh_m-values calculated using the Wilson–Geankoplis expression.

as steep as the (upward) slope in the large ν_i-range. The Sh_m-value in the $\nu_i \rightarrow 0$-limit is for the 2D pillar array case also significantly larger than in the case of the two considered 3D geometries (sphere array and TSM).

The best-fit equation is now given by:

$$Sh_m = \frac{20}{1 + 0.19\nu_i} + 7.6\nu_i^{0.18} (\varepsilon = 0.40) \quad 2 < \nu_i < 300 \qquad (13)$$

4.3. Use of calculated Sh_m-values for the prediction of the band broadening in chromatography

With the Sh_m-values calculated in an independent and correct (i.e., based on the local driving force) manner, it should be possible to apply Eq. (1) to predict the band broadening in chromatographic systems in a more accurate way than is possible when using the traditionally employed expressions of the form of Eq. (4), such as the Wilson and Geankoplis expression. To investigate this, the ability to use Eq. (1) in combination with the newly calculated Sh_m-data to model the highly accurate (numerically computed) plate height value sets for 2D pillar arrays and the TSM, respectively, presented by De Wilde et al. [19] and Detobel et al. [18], has been investigated.

Prior to this, the h_{inhom}-term appearing in Eq. (1) was first written in more explicit terms, using the Giddings-coupling theory [11]. Since only perfectly ordered systems are considered in the present study, only one Giddings-coupling term should be sufficient (short- or long-range coupling distances are not present in ordered systems), so that:

$$h_{inhom} = \frac{A\nu_i}{1 + D\nu_i} \qquad (14)$$

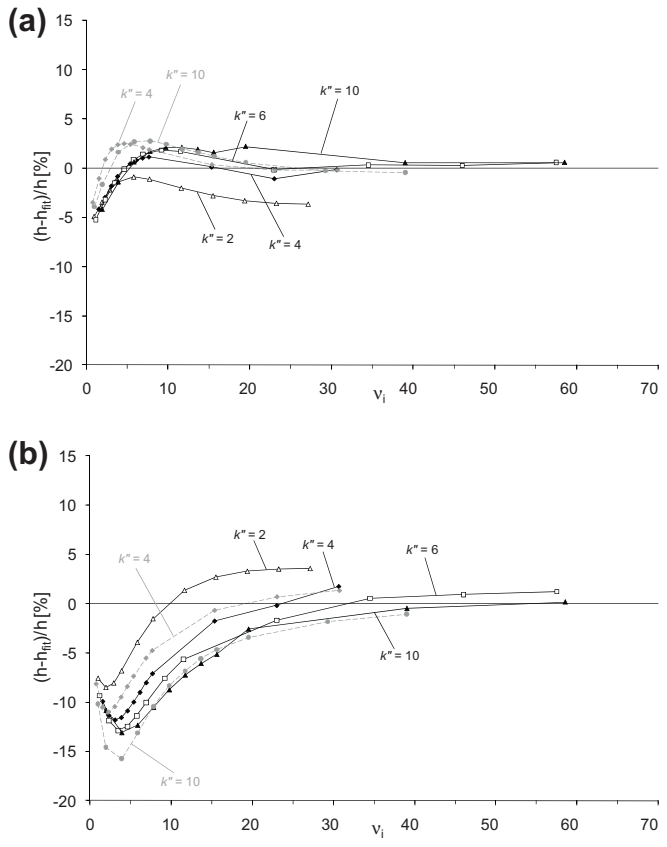

Fig. 10. Relative residual plots for the fitting quality of the TSM ($\varepsilon = 0.60$)-data shown in Fig. 7b using (a) the presently computed Sh_m-values and (b) Sh_m-values calculated using the Wilson–Geankoplis expression.

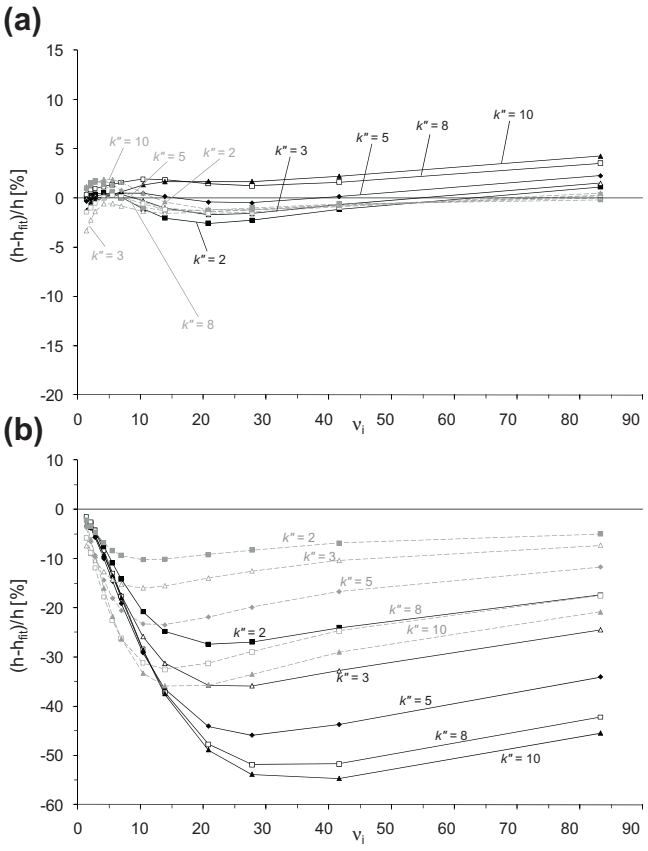

Fig. 11. Relative residual plots for the fitting quality of the 2D pillar array data shown in Fig. 8 using (a) the presently computed Sh_m-values and (b) Sh_m-values calculated using the Wilson–Geankoplis expression.

Using the Sh_m-data calculated in the present study, the only unknown coefficients in the set of expressions defined by Eqs. (1) and (14) are the A- and D-values needed in Eq. (14). This reduces the fitting problem from a 4-parameter fitting problem in [18,19] to only a 2-parameter fitting problem in the present study. This makes the fitting test considerably more demanding than the ones in [18,19], as there are now less fitting parameters that can absorb some of the modeling errors.

As can be noted from the excellent agreement between the plate height data and the best-fit curves in Figs. 7 and 8, the ability to model such a complex dependency on ν_i, k'' and D_{part} using only two fitting parameters (A and D, which are furthermore kept the same for every different case of D_{part} and k'') is striking. This holds for both the TSM-structures (Fig. 7) and the 2D pillar array data (Fig. 8).

Using the same approach, but now with the Wilson–Geankoplis expression to calculate Sh_m, the fitting quality is clearly less good, as can be noted from the relative residual plots given in Figs. 9–11 (compare panel (a) with panel (b) in each figure). All in all, the average relative residual fitting error reduces from resp. 3.5% (TSM with $\varepsilon = 0.38$), 6.9% (TSM with $\varepsilon = 0.60$) and 19% (2D pillar array) when using the Wilson–Geankoplis expression to resp. 1.2% (sphere array), 1.6% (TSM) and 1.0% (2D pillar array) when using the Sh_m-values computed in the present study.

Given the relative fitting errors are still reasonable, one could argue that the Wilson–Geankoplis-based plate height predictions are still relatively good (especially for the TSM-cases). It should, however, be considered that this relative good fit is obtained because the h_{inhom}-term partly make up for the errors induced by the Wilson–Geankoplis by distorting the best-fit A- and D-values. This, however, also implies that the use of a wrong Sh_m-correlation is bound to lead to errors on the observed eddy-dispersion.

5. Conclusions

The expressions for the mobile zone mass transfer coefficient (or its dimensionless variant, the Sherwood-number) that have up to now been traditionally used in the field of chromatography, such as the popular correlations of Wilson and Geankoplis [13], Kataoka et al. [39], are based on a measurement method neglecting the effect of the axial dispersion. As a consequence, these equations predict that the mass transfer term tends to zero when the velocity tends to zero ($Sh_m \to 0$ when $\nu_i \to 0$).

This behaviour deviates from the behaviour of the true mass transfer coefficient that should be used in the general plate height expression. The coefficient appearing there should be based on the local driving force (using the true local concentration) and not on the driving force estimated from the inlet and outlet concentrations only. In agreement with theory [22,28] and earlier experiments [21,22,26,27], this leads to much larger values of Sh_m. Depending on the considered geometry (spheres versus cylindrical pillars versus tetrahedral skeleton but all with an external porosity of the order of 40%), Sh_m is of the order of $Sh_m = 10$ to 20 in the range of reduced velocities below $\nu_i = 50$, hence including the range typically covered in liquid chromatography. These values are roughly some 2–5 times larger than those predicted by the Wilson and Geankoplis-correlation, which has up to now been the Sh_m-correlation that is used most often in liquid chromatography, but which is based on a wrongly defined driving force and which has been obtained in a range of reduced velocities ($\nu > 40$) that is too large for the field of liquid chromatography. The data represented in [21,22,26–28] are

based on the correct driving force, and are in full agreement with the data set obtained in the presently proposed numerical study.

Conducting an extensive series of computational fluid dynamics simulations and retrieving the Sh_m-data directly from the local value of the mass transfer flux (instead of using the traditional method based on Eq. (7), which underestimates the true mass transfer flux due to the neglect of axial dispersion), a set of new correlations describing the variation of the Sh_m-coefficient as a function of the reduced velocity has been established for the different considered geometries. These expressions show that the use of the Wilson–Geankoplis correlation, as well as the Kataoka- and the penetration-model in the field of liquid chromatography may need to be reconsidered. Future research efforts are needed to expand the correlations to more close representations of random sphere packings and provide the experimental validation for them.

References

[1] L. Lapidus, N.R.J. Amundson, Phys. Chem. 56 (1952) 984.
[2] J.J. van Deemter, F.J. Zuiderweg, A. Klinkenberg, Chem. Eng. Sci. 5 (1956) 271.
[3] J. Huber, J. Chromatogr. Sci. 7 (1969) 85.
[4] E. Kucera, J. Chromatogr. 19 (1965) 237.
[5] C. Horvath, H.-J. Lin, J. Chromatogr. 126 (1976) 401.
[6] F. Gritti, G. Guiochon, Anal. Chem. 78 (2006) 5329.
[7] A. Felinger, J. Chromatogr. A 1126 (2006) 120.
[8] G. Desmet, K. Broeckhoven, Anal. Chem. 80 (2008) 8076.
[9] G. Desmet, S. Deridder, J. Chromatogr. A 1218 (2011) 32.
[10] K. Miyabe, M. Ando, N. Ando, G. Guiochon, J. Chromatogr. A 1210 (2008) 60.
[11] J.C. Giddings, Dynamics of Chromatography. Part 1, Marcel Dekker, New York, 1965.
[12] P. Magnico, M. Martin, J. Chromatogr. A 571 (1990) 31.
[13] E.J. Wilson, C.J. Geankoplis, Ind. Eng. Chem. Fundam. 5 (1966) 9.
[14] F. Gritti, G. Guiochon, J. Chromatogr. A 1217 (2010) 5137.
[15] A. Cavazzini, F. Gritti, K. Kaczmarski, N. Marchetti, G. Guiochon, Anal. Chem. 79 (2007) 5972.
[16] G. Guiochon, J. Chromatogr. A 1168 (2007) 101.
[17] F. Gritti, G. Guiochon, J. Chromatogr. A 1216 (2009) 4752.
[18] F. Detobel, G. Desmet, Modeling chromatographic band broadening in monolithic columns, in: E. Machtejevas, N. Tanaka, K.K. Unger (Eds.), Monolithic Silicas in Separation Science: Concepts, Synthesis, Characterization, Modeling and Applications, VCH Wiley Verlag GmbH, Weinheim, 2011, pp. 105–126.
[19] D. De Wilde, F. Detobel, J. Billen, J. Deconinck, G. Desmet, J. Sep. Sci. 32 (2009) 4077.
[20] E. Papoutsakis, D. Ramkrishna, H.C. Lim, Appl. Sci. Res. 36 (1980) 13.
[21] P. Fedkiw, J. Newman, Chem. Eng. Sci. 33 (1978) 1043.
[22] P. Fedkiw, J. Newman, Int. J. Heat Mass Transfer 25 (1982) 935.
[23] N. Wakao, S. Kaguei, T. Funazkri, Chem. Eng. Sci. 34 (1978) 325.
[24] H.Y. Sohn, Lett. Heat Mass Transfer 4 (1977) 403.
[25] F. Gritti, G. Guiochon, J. Chromatogr. A 1218 (2011) 907.
[26] T. Miyauchi, T. Kikuchi, K.H. Hsu, Chem. Eng. Sci. 31 (1975) 493.
[27] D.J. Gunn, J.F.C. Souza, Chem. Eng. Sci. 29 (1974) 1363.
[28] R. Pfeffer, Ind. Eng. Chem. Fundam. 3 (1964) 380.
[29] G. Rexwinkel, A.B.M. Heesink, W.P.M. Swaaij, Chem. Eng. Sci. 52 (1997) 3995.
[30] P.P.H. Tock, P.P.E. Duijsters, J.C. Kraak, H. Poppe, J. Chromatogr. 506 (1990) 185.
[31] J.H. Knox, J. Chromatogr. Sci. 7 (1980) 453.
[32] W. De Malsche, H. Gardeniers, G. Desmet, Anal. Chem. 80 (2008) 5391.
[33] H. Eghbali, V. Verdoold, L. Vankeerbergen, J.G.E. Gardeniers, G. Desmet, Anal. Chem. 81 (2009) 705.
[34] F. Detobel, S. De Bruyne, J. Vangelooven, W. De Malsche, T. Aerts, H. Terryn, H. Gardeniers, S. Eeltink, G. Desmet, Anal. Chem. 82 (2010) 7208.
[35] N. Vervoort, P. Gzil, G.V. Baron, G. Desmet, Anal. Chem. 75 (2003) 843.
[36] N. Vervoort, P. Gzil, G.V. Baron, G. Desmet, J. Chromatogr. A 1030 (2004) 177.
[37] P. Gzil, N. Vervoort, G.V. Baron, G. Desmet, J. Sep. Sci. 27 (2004) 887.
[38] F.P. Incropera, D.P. DeWitt, Fundamentals of Heat and Mass Transfer, 5th ed., John Wiley & Sons, New York, 2002.
[39] T. Kataoka, H. Yoshida, K. Ueyama, J. Chem. Eng. Jpn. 5 (1972) 132.